Thermodynamic, Dynamic, and Structural Properties of Ionic Liquids Comprised of 1-Butyl-3-methylimidazolium Cation and Nitrate, Azide, or Dicyanamide Anions

Dmitry Bedrov* and Oleg Borodin

Wasatch Molecular Inc., 2141 St Mary's Drive, Salt Lake City, Utah 84108

Received: May 31, 2010; Revised Manuscript Received: August 31, 2010

Molecular dynamics simulations of ionic liquids (IL) comprised of 1-butyl-3-methylimidazolium [bmim] cation and nitrate [NO_3], azide [N_3], or dicyanamide [$N(CN)_2$] anions were conducted using the polarizable APPLE&P force field. Comparison of thermodynamic properties such as densities, enthalpies of vaporization, and ion binding energies as well as structural correlations obtained from simulations at atmospheric pressure and temperature range 298−393 K showed that IL with the $N(CN)_2$ anion shows significantly different characteristics as compared to ILs with the N_3 and NO_3 anions. [bmim][$N(CN)_2$] IL was found to have the lowest enthalpy of vaporization and the weakest ion−ion structural correlation as compared to ILs with the other two ions. This trend was further manifested in dynamical properties characterized by self-diffusion coefficients and molecular rotational relaxation times, where IL with the $N(CN)_2$ anion showed the fastest dynamics as compared to other ILs. We also examine the dynamic correlations between the ions' translational and rotational motions as well as discuss the anisotropy of the latter.

I. Introduction

Ionic liquids (ILs) are extensively investigated for a number of applications as potentially novel and environmentally friendly materials. Applications of ILs are extremely broad including solvents for synthetic and catalytic applications,[1] lubricants,[2,3] lithium batteries,[4−7] actuators,[8,9] sensors,[10] reaction media,[11] replacements for conventional solvents,[12] active pharmaceutical ingredients,[11] and explosives and propellants.[13−16] One of the advantages of ILs is the possibility to tailor an IL with desired properties through manipulation of a wide variety of cation and anion chemical structures and their combinations. While the empirical knowledge has been accumulated in numerous works reported in the literature, the fundamental molecular level understanding of correlations between the ions' structure or their combination and the bulk properties of ILs is still lacking.

In this work, we employ molecular dynamics (MD) simulations utilizing a highly accurate polarizable force field to systematically study the influence of the anion type on thermophysical, structural, and dynamical properties of 1-butyl-3-methylimidazolium [bmim]-based ILs. Specifically, we focus on the nitrogen-containing anions such as nitrate [NO_3], azide [N_3], and dicyanamide [$N(CN)_2$]. These ILs have been explored as novel energetic materials (explosives) and propellants. The ILs with these anions have been considered as novel hypergolic materials that can ignite spontaneously upon contact with an oxidizer.[13−15] Interestingly, it was found that the selection of anion plays a crucial role in determining whether an IL is hypergolic or not. For example, ILs containing nitrate or azide anions did not show hypergolic behavior upon contact with common oxidizers, while ILs comprised of the same cations and $N(CN)_2$ anion were found to be hypergolic. The hypergolic behavior of a material can, in principle, depend on a plethora of factors, including kinetics of chemical reactions with an oxidizer, interfacial properties between the oxidizer and the fuel, and processing conditions, etc. All of these factors might be crucial in defining the experimentally observed trends in hypergolicity of the above-mentioned ILs. However, before one can attempt to correlate any characteristics of ILs with their hypergolicity, a fundamental understanding of the influence of anion type on the basic bulk and interfacial properties of IL is needed. Understanding of the differences and similarities of [bmim][N_3], [bmim][NO_3], and [bmim][$N(CN)_2$] bulk properties is the subject of this Article, while the interfacial properties of these ILs will be discussed in future work. The selected anions have similar sizes (contain only 3−5 atoms), which is much smaller than the size of the bmim as can be seen from Figure 1 where the chemical structures of the ions are shown. Yet, as we show below, despite these similarities, the ILs containing these ions have very different properties.

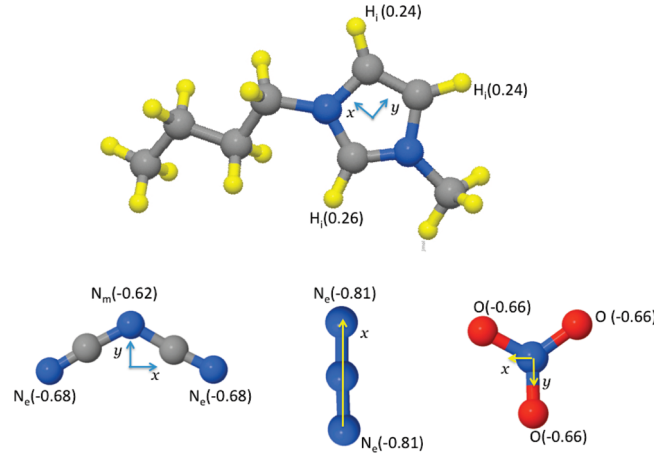

Figure 1. Molecular structure of ions used in simulations. Also shown are the labels and partial atomic charges for the selected atoms as well as the orientation and position of the local coordinate system for rotational dynamics analysis. Only *x* and *y* axes are shown; the *z*-axis is perpendicular to the *xy*-plane. Atoms coloring map: hydrogens, yellow; nitrogens, blue; carbons, gray; and oxygens, red.

Several MD simulations of some of these ILs have been already reported in the literature.[17−23] Wang and Voth used a

* Corresponding author. Phone: (801) 673-7452. Fax: (801) 581-4816. E-mail: bedrov@wasatchmolecular.com.

10.1021/jp1049827
Published on Web 09/17/2010

coarse-grained model to investigate spatial heterogeneities in alkyl imidazolium-based ILs with NO_3 anion.[22] These simulations showed that there is a significant alkyl tail aggregation in [bmim][NO_3] liquid. Micaelo et al. developed a united atom model for [bmim][NO_3] in the framework of GROMOS96 force field and conducted extensive simulations of this system as a function of temperature.[17] These simulations predicted density and viscosity of [bmim][NO_3] that are in very good agreement with experiment; however, the predicted enthalpy of vaporization of 130.2 kJ/mol at 298 K was about 32 kJ/mol lower than the experimental data later reported for this system by Emel'yanenko et al.[24] Cedena and Maginn used a fully atomistic model in their simulations of [bmim][NO_3].[23] These simulations also predicted liquid densities in very good agreement with experiment as well as provided a detailed analysis of structure and dynamics. Kowsari et al. investigated transport properties of [bmim]-based ILs with several anions including the [NO_3].[19,20] These studies consistently predicted much slower dynamics (characterized by self-diffusion coefficients, viscosities, and ionic conductivities) as compared to experiments for all ILs investigated. The only simulations of ILs with the $N(CN_2)_2$ anion that we are aware of are those conducted by the Steinhauser group for [emim][$N(CN)_2$] in which the structure, conductivity, and dielectric relaxation of the IL were investigated.[25−27]

Finally, we recently have reported MD simulations of a variety of ILs using the fully atomistic, polarizable APPLE&P force field that has been developed and extensively validated on a variety of substances including ILs.[28] This force field showed very good accuracy in describing the thermophysical and dynamical properties for various ILs using a transferable set of nonbonded interactions. MD simulations using the APPLE&P force field showed good agreement with experimental conductivities and viscosities for [bmim][$N(CN)_2$] and related ILs; however, those simulations predicted density for [bmim]-[$N(CN)_2$] that was about 2.0% lower than the reported experimental values. For [bmim][NO_3], simulations using this force field accurately reproduced reported experimental densities as a function of temperature, but overestimated the viscosity by almost a factor of 2 as compared to experiment. To the best of our knowledge, no simulations of ILs with bmim or other imidazolium-based cations and N_3 anion have been reported in the literature.

II. Simulation Details

Subsequently to the publication of the original version of the APPLE&P force field,[28] the parameters for $N(CN)_2$ and NO_3 anions were revised to improve the agreement with available experimental data in the liquid phase as well as description of crystal structures of closely related ILs containing these anions.[29] In this work, we used the revised APPLE&P potential, and therefore some data reported here are slightly different from the values reported in ref 28. Also, recently, the APPLE&P force field has been expanded to include ILs containing azide anions. While we are not aware of any experimental measurements on the [bmim][N_3] system, validation on closely related IL ([bmmim]-[N_3]) indicated that the force field accurately predicts the IL conductivity (within 30%) and density (within 1%) as compared to experimental values. The crystal structure of the 1-(2-butynyl)-3-methyl-immidazolium azide was also found to be in a good agreement with experiments.[30]

MD simulations of bulk [bmim][NO_3], [bmim][N_3], and [bmim][$N(CN)_2$] ILs have been conducted at 298, 333, and 393 K and atmospheric pressure. Each system contained 150 ionic pairs. MD simulations were conducted using the molecular simulation package Lucretius,[31] which has the capability to handle polarization effects. Covalent bond lengths were constrained using the velocity-Verlet form of the SHAKE algorithm.[32] The Ewald summation method was used for treatment of long-range electrostatic forces between partial atomic charges and between partial charges and induced dipoles. A tapering function was used to drive the induced dipole/induced dipole interactions to zero at the cutoff of 10 Å, with scaling starting at 9.3 Å. (The form of the tapering function is given in the Supporting Information.) Induced dipoles were calculated via a direct iteration with a predictor corrector method. A cutoff of 10 Å was used for all van der Waals interactions and the real part of electrostatic interactions in the Ewald summation. A multiple time step reversible reference system propagator algorithm[33] was employed. A time step of 0.5 fs was used for bonding, bending, dihedral, and out-of-plane deformation motions, while a 1.5 fs time step was used for nonbonded interactions within a cutoff radius of 6.0 Å. Finally, the nonbonded interactions in the range between 6.0 and 10.0 Å and reciprocal part of electrostatic interactions were updated every 3 fs. Each system was initially equilibrated in the NPT ensemble for at least 1 ns, while production runs ranged from 5 to 20 ns depending on the system and temperature. The length of the production run was chosen to be long enough to allow molecules to reach a diffusive regime (when the ion mean-squared displacement shows a linear time dependence, MSD(t) $\approx t$), therefore allowing an accurate estimation of the self-diffusion coefficients.

To calculate the enthalpy of vaporization, an ensemble of 150 ion pairs in a gas phase has been simulated using Brownian dynamics simulations. In these simulations, ions in a given (predefined) pair were allowed to interact only with each other, while any interactions with other ion pairs were turned off. All nonbonded interactions (van der Waals and electrostatic) were directly calculated for all possible pairwise interactions without any cutoff radius. Polarization effects were calculated taking into account only the electrostatic field created by the ionic pair. The duration of these simulations was over 1 ns, allowing accurate sampling of total energy per ion pair in the gas phase. Finally, to get the binding energy of the ionic pair, a gas-phase simulation of noninteracting (isolated) ions has been also conducted in which only intramolecular interactions were allowed.

III. Results and Discussion

A. Thermodynamic Properties. The [bmim][NO_3], [bmim]-[N_3], and [bmim][$N(CN)_2$] ILs' density, molar volume of ionic pair in the liquid, V_m, enthalpy of vaporization per ion pair, H_{vap}, and ion pair binding energy, $E_{\pm}$, are reported in Table 1 for several temperatures. Examination of Table 1 reveals the following trend for densities $\rho_{[bmim][NO3]} > \rho_{[bmim][N3]} > \rho_{[bmim][N(CN)2]}$ with about 10% difference between the most and the least dense ILs. Table 1 also shows that MD simulations using APPLE&P force field predict densities that are within 1% of the experimental data reported in the literature[34−36] (shown in parentheses). In the temperature range investigated, the molar volumes per ionic pair were found to have a linear temperature dependence. The coefficients of thermal expansion defined as $\alpha = (dV/dT)/V$) were found to be 5.97×10^{-4}, 5.47×10^{-4}, and 5.94×10^{-4} for [bmim][$N(CN)_2$], [bmim][N_3], and [bmim][NO_3], respectively, at 333 K.

The enthalpy of vaporization has been calculated as

$$H_{vap} = E_{gas,pair} - E_{liq} + RT \quad (1)$$

TABLE 1: Density, Molar Volume per Ion Pair, Enthalpy of Vaporization, and Binding Energy of Ionic Pair As Obtained from MD Simulations Using the APPLE&P Force Field[a]

IL	T (K)	ρ (kg/m^3)	V_m (cm^3/mol)	H_{vap} (kJ/mol)	$E_\pm$ (kJ/mol)
[bmim][N(CN)$_2$]	298	1049.7 (1058[b])	195.3	132.6 (157.2[f]) (153.4[f]) (174[g])	366.5
	333	1028.2 (1041[b])	199.4	128.9	365.3
	393	992.2	206.6	122.9	363.2
[bmim][N$_3$]	298	1073.2	168.7	154.9	389.9
	333	1053.4	171.8	151.3	388.7
	393	1019.1	177.6	145.2	386.8
[bmim][NO$_3$]	298	1159.9 (1154[c])	173.3	145.8 (162.4[e])	387.0
	333	1135.6 (1131[c]) (1136[d])	177.0	142.2	386.2
	393	1097.4 (1092[c])	183.3	136.2	384.6

[a] Values in parentheses are experimental data available in the literature. [b] Reference 34. [c] Reference 35. [d] Reference 36. [e] Reference 24. [f] Reference 37. [g] Reference 38.

where E_{liq} is the total energy per mole of ion pairs in the liquid, $E_{gas,pair}$ is the total ion pair energy in the gas phase, R is the universal gas constant, and T is temperature. We found that the enthalpies of vaporization followed a slightly different trend than the densities. While [bmim][N(CN)$_2$] showed the lowest H_{vap}, the highest H_{vap} was obtained for [bmim][N$_3$]. Comparison of simulation enthalpies of vaporization with experimental data is not straightforward because experimental enthalpy of vaporization is one of the hardest thermodynamic properties to measure due to the negligible vapor pressure of the ILs. Experimental measurements often have to be conducted at elevated temperatures (to attain a reasonable vapor pressure) where chemical stability of ILs might become a point of concern. In Table 1 we show available experimental data for H_{vap} for the [bmim][NO$_3$][24] and [bmim][N(CN)$_2$][37] as obtained using a combined approach of combustion calorimetry and high-level quantum chemistry calculations,[24] and by ion pair fragmentation spectroscopy.[38] The simulation predicted values of H_{vap} are about 15 kJ/mol lower for both ILs. Similar underestimation of H_{vap} values predicted from simulations using APPLE&P force field has been observed in our previous studies of these and other ILs. However, for [bmim][NO$_3$], our simulations gave a value for H_{vap} of 145.8 kJ/mol, which is in good agreement with experiment (162.4 kJ/mol). In comparison, simulations using the united atom model of Micaelo et al.[17] predicted a value of 130.2 kJ/mol, while simulations using the OPLS-AA force field[18] gave a value of 117 kJ/mol when using the generic version of the force field, and 133 kJ/mol with the force field specifically adjusted for [bmim][NO$_3$].

Because of the difficulty of measuring the enthalpy of vaporization of ILs, several empirical correlations have been developed to predict this property. Recently, Verevkin has examined two of such empirical correlations for a number of ILs.[39] In that work, Verevkin proposed an empirical correlation between the H_{vap} and the chemical structure of IL using available experimental data for several ILs. In his approach, each atom type contributes a certain amount of enthalpy to the H_{vap}, as well as there are some additional structural corrections (i.e., for the ring structure in pyrrolidine moieties or for the CF$_3$ group). Verevkin used 12 different ILs, including [bmim][N(CN)$_2$], to fit these empirical contributions and then demonstrated that this contribution approach works reasonably well for several other ILs. The latter included [bmim][NO$_3$] for which Verevkin's correlation predicted $H_{vap} = 169.7$ kJ/mol, which is somewhat higher than the value of 162.4 kJ/mol obtained from combination of combustion calorimetry and ab initio calculations.[24] To the best of our knowledge, no experimental data for H_{vap} of [bmim][N$_3$] have been reported in the literature. Therefore, the predicted from our simulations values for H_{vap} of [bmim][N$_3$] can only be compared to the value obtained using the Verevkin's correlation. According to this correlation, the H_{vap} for [bmim][N$_3$] is 151.5 kJ/mol, which is 5 kJ/mol lower than the value of 156.5 kJ/mol obtained for the [bmim][N(CN)$_2$]. Quantitatively, this value of H_{vap} for the [bmim][N$_3$] is similar to the value of 154.9 kJ/mol predicted from our simulations at 298 K (see Table 1). However, in comparison with the other two ILs, predictions from Verevkin correlation are qualitatively different from the results of our simulations. In our simulations, the [bmim][N$_3$] has the largest value for H_{vap}, which is about 24 kJ/mol greater than the value for [bmim][N(CN)$_2$]. In contrast, the Verevkin correlation predicts that H_{vap} for [bmim][N$_3$] should be the lowest out of the three ILs investigated here and have a value very similar to that of [bmim][N(CN)$_2$]. Implications and validity of these qualitative trends are further discussed below in light of other properties obtained for these ILs.

Finally, from our simulations, we also calculated the ion pair binding energy defined as

$$E_\pm = E_{gas,isolated} - E_{gas,pair} \quad (2)$$

where $E_{gas,isolated}$ is a combined energy of isolated, noninteracting with each other cation and anion in a gas phase. Therefore, while H_{vap} represents the amount of energy required to evaporate an ionic pair from the liquid phase, the $E_\pm$ shows the energy necessary to separate (to infinite distance) two ions in the gas phase. Table 1 shows that the $E_\pm$ obtained from our simulations qualitatively follows the same trend as H_{vap}, that is, [bmim][N$_3$] showing the largest binding energy and [bmim][N(CN)$_2$] the lowest. The validity of this trend is supported by the ion pair binding energies obtained from high-level quantum chemistry (QC) calculations between 1-ethyl-3-methylimidazolium (emim) and the three anions investigated in this work. In Table 2 we compare binding energies obtained from QC calculations at the M05-2X/cc-pvTz level with those obtained from molecular mechanics (MM) calculations using the APPLE&P force field. Optimal geometries of ion pairs from these calculations are shown in the Supporting Information. The APPLE&P predictions show very good agreement with the QC results, further validating the accuracy of our force field. Also, the binding energies obtained from QC calculations for emim−anion pairs show the same trend as those for bmim−anion pairs reported in Table 1. Taking this into account, we believe that trends predicted for H_{vap} using APPLE&P are more reliable than those obtained from Verevkin correlation.

TABLE 2: Cation−Anion Binding Energies (in kJ/mol) As Obtained from Quantum Chemistry (QC) Calculations (at the M05-2X/cc-pvTz Level) and Molecular Mechanics Using APPLE&P Force Field[a]

ion pair	QC	APPLE&P
[emim][DCA],geom1[b]	366	379
[emim][DCA],geom2	359	376
[emim][N_3]	410	402
[emim][NO_3]	403	396

[a] Binding energies defined as $E_{\text{isolated ions}} - E_{\text{pair}}$. [b] Two geometries with similar energies were investigated for [emim][$N(CN)_2$]. Pictures and *XYZ* coordinates of optimized geometries are given in the Supporting Information.

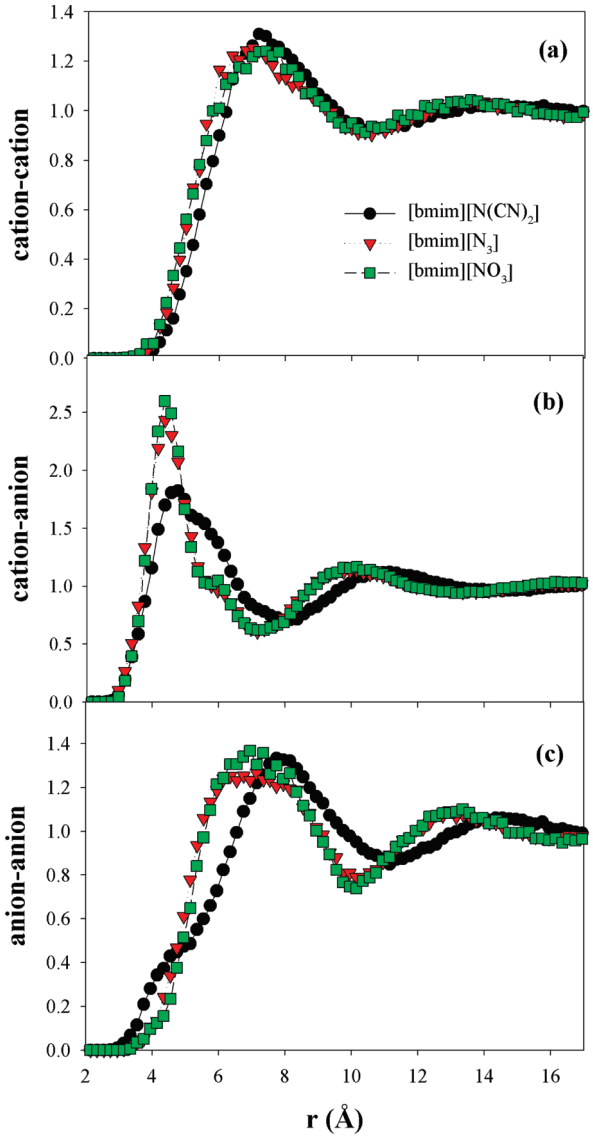

Figure 2. Ion−ion center-of-mass radial distribution functions as obtained from MD simulations of three ILs at 333 K.

B. Structure. To understand the influence of anion type on IL structure, several structural correlations were analyzed using the trajectories obtained from our simulations. In Figure 2, the cation−cation, cation−anion, and anion−anion center-of-mass radial distribution functions, $g(r)$, are compared at 333 K for the three ILs investigated. This figure clearly shows that, while the cation−cation correlations are quite similar for all three ILs, the cation−anion and anion−anion $g(r)$ values for [bmim]-[$N(CN)_2$] are significantly different from the corresponding

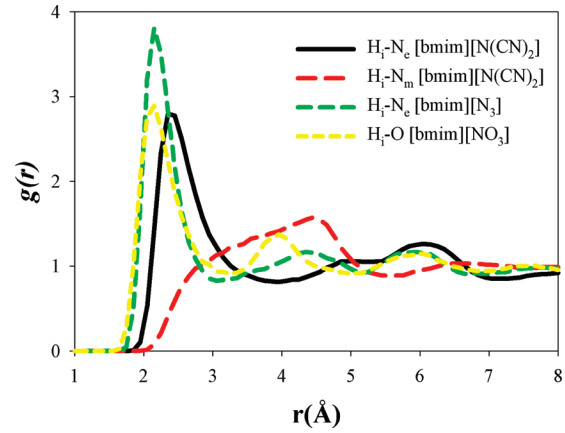

Figure 3. Radial distribution functions between hydrogens on imidazolium ring and anion atoms with large negative partial atomic charges (see Figure 1 for label notation).

correlations in [bmim][N_3] and [bmim][NO_3], both of which have $g(r)$'s that are similar to each other. As can be seen from Figure 2b, the first peak of cation−anion $g(r)$ in [bmim][$N(CN)_2$] is significantly smaller and broader than the almost identical peaks in [bmim][N_3] and [bmim][NO_3], indicating a weaker structural correlation between cation and anion centers-of-mass. The latter seems to be consistent with the weaker binding energy and lower enthalpy of vaporization obtained for [bmim][$N(CN)_2$] (see Table 1 and discussion above). The anion−anion $g(r)$ for [bmim][$N(CN)_2$] also shows noticeably different behavior as compared to $g(r)$ in [bmim][N_3] and [bmim][NO_3] as illustrated in Figure 2c. At short separations (<4.5 Å), the anion−anion $g(r)$ in [bmim][$N(CN)_2$] is larger than that for the other two anions, indicating that, despite its larger size, the $N(CN)_2$ anions can easily approach each other in some configurations. Yet, the position of the first peak for the $N(CN)_2$ anion−anion $g(r)$ is shifted to larger distances (∼8 Å) as compared to the peak positions for N_3 and NO_3 anions (∼6.5−7.0 Å). For [bmim]-[NO_3], the position and the relative heights of the first and second peaks for all three $g(r)$ values obtained from our simulations are in very good agreement with those reported by Cedena and Maginn using atomistic simulations with nonpolarizable force field.[23] Also, our center-of-mass $g(r)$ values for [bmim][$N(CN)_2$] are similar to those reported by Schroder et al.[17] for [emim][$N(CN)_2$].

We continue the comparison of structural correlations by examining atomistic intermolecular pair distribution functions. Specifically, in Figure 3 we show $g(r)$ values between hydrogens on imidazolium ring (H_i) and anion atoms that have large negative partial atomic charges and, therefore, experience strong electrostatic interaction (i.e., "hydrogen bonding") with imidazolium hydrogen atoms. In Figure 1 the labels and the values of partial atomic charges are given for atoms for which $g(r)$ was calculated. Figure 3 shows that H_i-N_e $g(r)$ in [bmim][N_3] and H_i-O $g(r)$ in [bmim][NO_3] have a strong first peak at separation around 2.1 Å, typical of hydrogen bonding. The first peak in the [bmim][N_3] H_i-N_e $g(r)$ is about 30% higher than in the [bmim][NO_3] H_i-O $g(r)$; however, this does not mean that bmim on average makes more hydrogen bonds with N_3 than with NO_3 anion. IL with NO_3 has a higher number density of atoms capable of forming hydrogen bonds with bmim (the three oxygens of NO_3) as compared to that in the [bmim][N_3] (where only two nitrogens on azide ends can participate in the hydrogen bonding). Note that the partial atomic charge of the middle nitrogen in azide has a relatively large positive value and, hence, cannot favorably interact with bmim hydrogens.

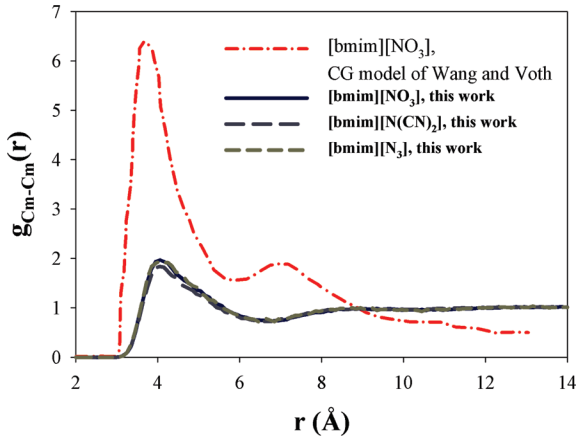

Figure 4. Radial distribution functions between the butyl methyl groups as obtained from our simulations of [bmim][NO_3],[bmim][N_3], and [bmim][$N(CN)_2$] at 393 K. Also shown is the corresponding $g(r)$ obtained from the coarse-grained simulations of [bmim][NO_3] by Wang and Voth (extracted from ref 22).

Therefore, to compare the number of hydrogen bonds formed in each IL, we calculated the coordination number (N_c) within the first coordination shell of imidazolium hydrogens defined as a sphere of 3.0 Å (corresponds to the position of the first minimum in H_i-O and H_i-N_e $g(r)$ in [bmim][NO_3] and [bmim][N_3], respectively). These calculations reveal that within a sphere of 3.0 Å radius, the imidazolium hydrogen has on average 1.6 oxygen atoms of NO_3 and 1.2 nitrogen atoms of N_3 in [bmim][NO_3] and [bmim][N_3], respectively. Although one needs to remember that, due to its chemical structure, the NO_3 anion could easily orient itself such that two of its oxygens favorably interact with the same bmim hydrogen, while N_3 can only contribute one nitrogen for a given hydrogen bond. Finally, the $N(CN)_2$ anion has three nitrogen atoms with large negative partial charges as shown in Figure 1, and hence, in principle, all of them can form hydrogen bonds with bmim. Nevertheless, we calculated separately the $g(r)$ between the bmim hydrogens and the end (N_e) and middle (N_m) nitrogens of $N(CN)_2$. Figure 3 clearly shows that while the H_i-N_e $g(r)$ in [bmim][$N(CN)_2$] has a well-defined first peak, similar to those seen for N_3 and NO_3 anions, the H_i-N_m $g(r)$ shows no signs of strong favorable interaction between anion middle nitrogen and bmim hydrogens. In this IL, the bmim H_i on average has about 1.0 N_e and 0.2 N_m nitrogens of $N(CN)_2$ in a sphere of 3.0 Å radius.

We also analyzed the tendency of alkyl tails of bmim to segregate into domains. In their simulations of [bmim][NO_3] using coarse-grained model, Voth and Wang reported a strong aggregation of end-groups of the bmim butyl tails, an indication of a strong spatial heterogeneity in alkyl-imidazolium-based ILs.[22] We have conducted a similar analysis and in Figure 4 show $g(r)$ for the methyl carbons on the bmim butyl tail as obtained from our simulations at 393 K. For the three ILs investigated, the butyl end-groups do not show any more structural correlation than, for example, the cation−anion $g(r)$ shown in Figure 2b. Indeed, the first peak in the butyl methyl−butyl methyl $g(r)$ reaches values of 1.8−1.9, indicating an increased correlation between butyl end-groups at short separations; however, at larger separations $r > 8$ Å, the $g(r)$ does not deviate much from unity, indicating a homogeneous distribution of the end-groups. For comparison, we also show the corresponding $g(r)$ extracted from ref 22, which clearly shows a qualitatively different behavior despite the fact that it has been obtained from simulations at a much higher temperature (700 K) where spatial correlations are expected to be weaker than at 393 K. Taking into account such qualitative difference between our $g(r)$ and those from ref 22, we believe that the coarse-grained model used by Voth and Wang greatly overestimated the aggregation between the alkyl tails, and, hence, the structural heterogeneities reported in that work are over exaggerated.

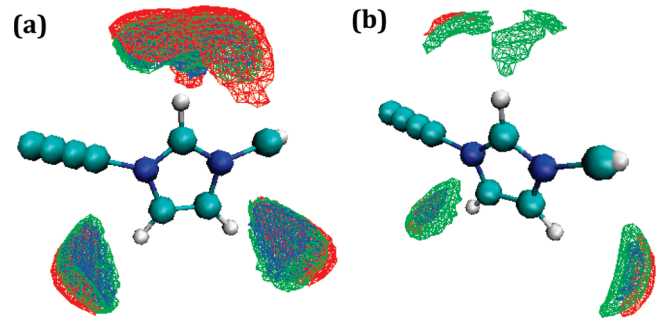

Figure 5. 3D distributions of $\rho_i/\langle\rho\rangle$ isosurfaces for N_e (in N_3 and $N(CN)_2$) and O (in NO_3) atoms around bmim: (a) $\rho_i/\langle\rho\rangle = 10.0$, (b) $\rho_i/\langle\rho\rangle = 18.0$. Red, [bmim][$N(CN)_2$]; green, [bmim][$N_3$]; and blue, [bmim][$NO_3$].

We conclude our analysis of structural correlations with three-dimensional (3D) density distributions of anion atoms around the cation. In this analysis, the three carbon atoms on imidazolium ring defined one of the coordinate system planes. The simulation box was divided into lattice cells of size 0.4 Å, and the relative density distribution $\rho_i/\langle\rho\rangle$, where ρ_i is the local number density of atoms of interest in the ith lattice cell and $\langle\rho\rangle$ is the average number density of these atoms in the system, was calculated by averaging over all bmim molecules and the entire trajectory. First, we compare these 3D distributions for anion atoms that form hydrogen bonding with bmim H_i atoms, that is, N_e in [bmim][N_3] and [bmim][$N(CN)_2$] and O in [bmim][NO_3]. At 333 K, the maximum values of $\rho_i/\langle\rho\rangle$ were found to be 25.4 and 40.0 for N_e in [bmim][N_3] and [bmim][$N(CN)_2$], respectively, and 24.8 for O in [bmim][NO_3]. In Figure 5 isosurfaces for $\rho_i/\langle\rho\rangle = 10.0$ (Figure 5a) and 18.0 (Figure 5b) are shown for these distributions. These isosurfaces have relatively high values of local density (as compared to the bulk average) and therefore represent relatively low free energy configurations that frequently occur during simulations. At $\rho_i/\langle\rho\rangle = 10.0$, distributions for all three ILs are very similar, showing three well-defined regions of preferable location of hydrogen-bonding atoms, which are found to be in the vicinity of bmim H_i. These locations are also similar to the preferred locations of Ntf_2 anion oxygen atoms,[40] further indicating the similarity of the bmim cation coordination by various anions. The similarity of distributions observed in Figure 5a indicates that for a given cation (bmim), the anion type does not influence the distribution of preferable locations of anion atoms that participate in hydrogen bonding. On the other hand, the maximum values of $\rho_i/\langle\rho\rangle$ reported above indicate that, despite the fact that $\langle\rho\rangle$ of $N(CN)_2$ N_e atoms is about 10% lower than that for N_e of N_3 (due to difference in overall density of [bmim][$N(CN)_2$] and [bmim][N_3]), the maximum value of $\rho_i/\langle\rho\rangle$ for the latter is almost 2 times larger. This indicates that there are certain locations around the bmim cation in which nitrogens at N_3 ends have significantly lower free energy as compared to those on $N(CN)_2$ ends. Isosurfaces for higher density ($\rho_i/\langle\rho\rangle = 18.0$, Figure 5b) show that the region above the bmim N−C−N bend is less favorable than the other two regions on the other side of the bmim ring where anion atoms can form hydrogen bonds without steric interference from the

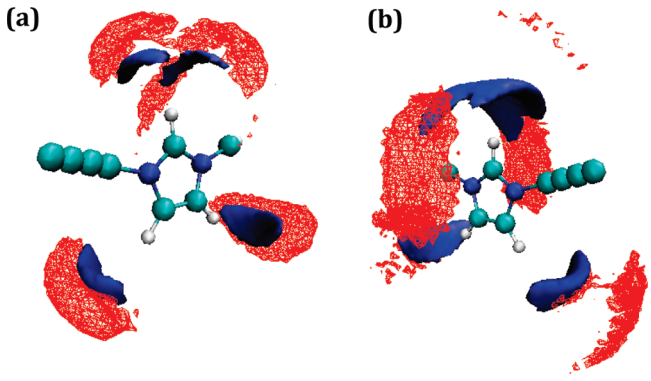

Figure 6. 3D distributions of $\rho_i/\langle\rho\rangle$ isosurfaces for N_e and N_m atoms around bmim: (a) in [bmim][N_3] solid, $\rho_{Ne}/\langle\rho_{Ne}\rangle = 17.0$ ($\max(\rho_{Ne}/\langle\rho_{Ne}\rangle) = 40.0$), wire frame: $\rho_{Nm}/\langle\rho_{Nm}\rangle = 10.0$ ($\max(\rho_{Nm}/\langle\rho_{Nm}\rangle) = 24.0$); (b) in [bmim][$N(CN)_2$] solid, $\rho_{Ne}/\langle\rho_{Ne}\rangle = 10.0$ ($\max(\rho_{Ne}/\langle\rho_{Ne}\rangle) = 25.2$), wire frame: $\rho_{Nm}/\langle\rho_{Nm}\rangle = 4.5$ ($\max(\rho_{Nm}/\langle\rho_{Nm}\rangle) = 9.1$).

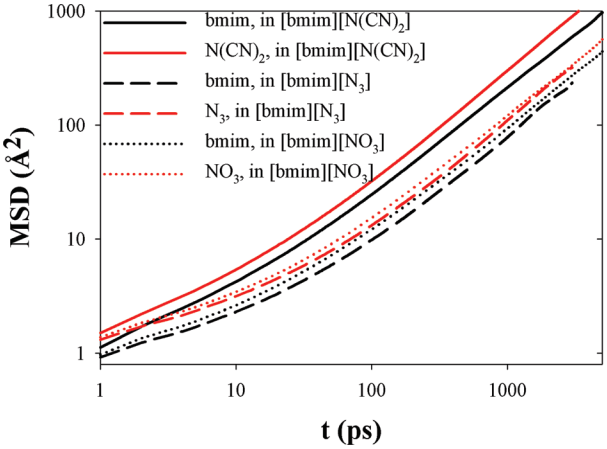

Figure 7. Mean-squared displacements (MSD) of ions as a function of time obtained from simulations of [bmim][NO_3], [bmim][N_3], and [bmim][$N(CN)_2$] at 393 K.

methyl and butyl groups and where the maximum values in $\rho_i/\langle\rho\rangle$ were found for all anions investigated here.

3D-distributions can also be helpful in understanding the relative orientation of anions in the first coordination shell of bmim. While for the relatively symmetric NO_3 anion its relative orientation is not particularly interesting, the orientation of N_3 and $N(CN)_2$ anions can be gleaned from the analysis of Figure 6 where the 3D-distributions of end and middle nitrogens are compared for the same anion. Figure 6a shows that the distributions of N_e and N_m nitrogens of N_3 are basically parallel to each other, indicating that the longest dimension of the N_3 anion is almost aligned along the H_i-N_e hydrogen bond. On the other hand, isosurfaces for N_m and N_e of $N(CN)_2$ are shifted relative to each other as can be seen from Figure 6b. The relative location of these isosurfaces is consistent with configurations in which the $N(CN)_2$ anion can form two hydrogen bonds with the same bmim: one with H_i on the N−C−N bend and another with H_i on the opposite side of imidazolium ring.

C. Dynamical Properties. We begin our analysis of dynamical properties with comparison of self-diffusion coefficients (D) of ions as a function of temperature. To obtain the self-diffusion coefficient, mean-squared displacements (MSDs) for each ion type were calculated as a function of time and are shown in Figure 7 at 393 K. For all three ILs at any given time t, the anion has a larger MSD as compared to bmim, which is expected taking into account that all anions investigated here are smaller than bmim cation. Figure 7 clearly shows that anion

TABLE 3: Ion Self-Diffusion Coefficients Obtained from MD Simulations at Various Temperatures, and Ratios between the Anion and Cation Self-Diffusion Coefficients and Ionic Conductivity[a]

		D (10^{-10} m^2/s)			
IL	T (K)	cation	anion	D_{an}/D_{cat}	λ mS/cm
[bmim][$N(CN)_2$]	298	0.30	0.41	1.37	8.9 (11[b])
	333	1.07	1.50	1.40	28.4 (24.1[b])
	393	3.21	4.95	1.54	73.7
[bmim][NO_3]	298	0.058	0.066	1.14	1.7
	333	0.29	0.37	1.27	8.0
	393	1.50	1.90	1.27	32.8
[bmim][N_3]	298	0.020	0.023	1.15	0.65
	333	0.15	0.17	1.13	4.1
	393	1.11	1.38	1.24	26.8

[a] Where available, experimental data are shown in parentheses. [b] Reference 45.

type has a significant influence on the mobility of ions in ILs. While ion MSDs in [bmim][N_3] and [bmim][NO_3] are similar, with somewhat systematically higher MSD for the latter, the ion mobility in [bmim][$N(CN)_2$] is significantly larger than in the other two ILs. To obtain the self-diffusion coefficients, the MSD(t) values were fitted as a linear function of time (t) for data where MSD(t) > 10.0 Å^2. The latter condition ensures that the fitting is done for the time scales on which ion motion is diffusive. In Table 3 the ion self-diffusion coefficients obtained in this way are given for three ILs at three temperatures investigated. Consistent with MSD shown in Figure 7, the obtained self-diffusion coefficients in [bmim][$N(CN)_2$] are significantly higher than for the other two ILs. At 298 K, the mobility of both ions in [bmim][N_3] is an order of magnitude slower than that in the [bmim][$N(CN)_2$]. At 393 K, the difference between ion self-diffusion coefficients in these ILs reduces but still is about a factor of 3 different. Ratios of the anion and cation self-diffusion coefficients in the same IL are also given in Table 3. These show a strong correlation between the cation and anion mobilities. The self-diffusion coefficient of anions is only 15−30% higher than that for bmim in [bmim][NO_3] and [bmim][N_3]. In [bmim][$N(CN)_2$], the difference between ions mobilities is about 40−50%. Interestingly, both simulations using nonpolarizable force fields[17,23] predicted that the self-diffusion of NO_3 in [bmim][NO_3] is slightly (10−20%) slower than that of bmim, which seems surprising taking into account the difference in bmim and NO_3 sizes.

In our recent paper,[40] we showed that empirical correlations between the ions' average self-diffusion coefficient and thermodynamic properties of IL work reasonably well for a wide variety of ILs. Specifically, correlations relating D with the H_{vap}, $E_{\pm}$, and V_m have been suggested. In Figure 8 we demonstrate one of these correlations $-\log(D) \approx H_{vap} + 0.18E_{\pm}$ for several ILs that contain bmim cation and have been simulated using the APPLE&P force field, including those simulated in this work. As can bee seen from Figure 8, the data for [bmim][N_3] follow this empirical correlation very well, further indicating that our relatively high values of H_{vap} are consistent with the slow dynamics in this system. No direct measurements of the ion mobility in [bmim][N_3] have been reported in the literature; however, there are a couple indirect cases of evidence that the noticeably slower dynamics in this IL can be expected as compared to ILs with other anions. In ref 15, a value of 404 cP at 298 K has been reported for viscosity of a supercooled [bmim][N_3] liquid, which is about a factor of 2 larger than the experimental data for [bmim][NO_3].[35] Also, a recent study of [bmmim]-based ILs and mixtures with N_3 and BF_4 anions[41]

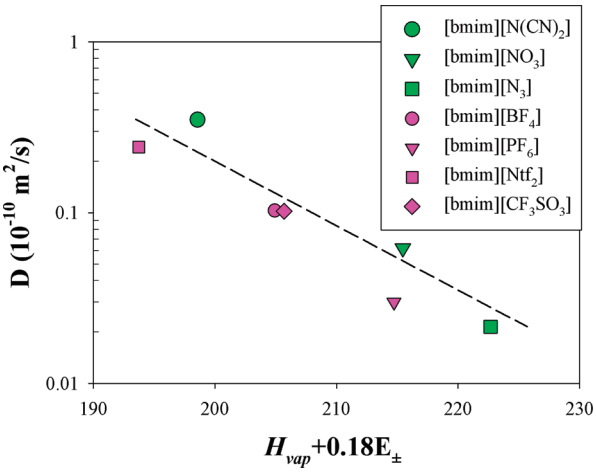

Figure 8. Correlation between the average ion self-diffusion coefficient and the enthalpy of vaporization (H_{vap}) and the cation−anion binding energy $E_{\pm}$ as obtained from MD simulations using APPLE&P force field for various ILs with bmim cation at 298 K. Data include three ILs investigated here and those reported in ref 40.

showed that at 313 K, IL with the N_3 anion had about 60% higher viscosity than the IL with the BF_4 anion. Taking into account the consistency of simulation data with empirical correlation in Figure 8 as well as experimental data on related systems mentioned above, we believe that both thermodynamic and dynamic properties predicted from our simulations for [bmim][N_3] are quite reasonable.

We also analyzed the rotational dynamics of ions as a function of temperature. In this analysis, for all ions, except the N_3, a local coordinate system was defined, and a rotational autocorrelation function (ACF) for each unit vector $\mathbf{e}_i$ ($i = \{x,y,z\}$) defining this local coordinate system was calculated as:

$$\mathrm{ACF}_i(t) = \langle[\mathbf{e}_i(0)\cdot\mathbf{e}_i(t)]\rangle \quad (3)$$

where $\mathbf{e}_i(0)$ and $\mathbf{e}_i(t)$ are the values of the unit vectors at time zero and t, respectively, while brackets denote an ensemble average over all molecules of the same type and time origins. The location of the origin and orientation of the selected local coordinate system for each molecule are given in Figure 1. For the N_3 anion, a vector between two nitrogen atoms on the molecule ends was considered instead of rotation of the local coordinate system. The obtained ACFs were fitted with Kohlrausch−Williams−Watts (KWW) function given by:

$$P_{\mathrm{KWW}}(t) = A\exp(-(t/t_r)^{\beta}) \quad (4)$$

where t_r is a relaxation time parameter, parameter β determines the degree of stretching and characterizes the broadness of the relaxation process, and prefactor A allows us to account for the decay that occurs on time scales faster than 1 ps^{-1}. Rotational relaxation times (τ) were obtained by integrating eq 4 over time from zero to infinity and are given in Table 4.

Examination of Table 4 reveals several interesting observations. Rotation of bmim in all ILs is quite anisotropic. Relaxation of the x-axis, which is aligned along the largest dimension of bmim molecule, is about a factor of 3−4 slower than the relaxation of the other two axes for which the reorientation of the butyl tail is not required. As with the self-diffusion coefficient, the slowest rotation of all axes is observed for bmim in [bmim][N_3], while the fastest is seen in [bmim][$N(CN)_2$].

TABLE 4: Rotational Relaxation Times in picoseconds Obtained from MD Simulations at Various Temperatures[a]

		cation			anion		
IL	T (K)	τ_x	τ_y	τ_z	τ_x	τ_y	τ_z
[bmim][$N(CN)_2$]	298	1036	315	332	251	37.3	28.9
	333	299	96.6	101	77.4	7.8	6.2
	393	90.8	28.3	29.1	24.2	1.9	1.7
[bmim][NO_3]	298	4588	1808	1925	5.1	5.1	8.0
	333	1134	402	387	3.1	3.1	3.9
	393	200	75.6	77.2	1.7	1.7	1.9
[bmim][N_3]	298	26 489	4120	4130	99.9		
	333	2415	684	753	26.8		
	393	243	92.0	91.4	6.7		

[a] See text and Figure 1 for definition of the x, y, and z axes.

The rotation of the $N(CN)_2$ anion is also quite anisotropic with relaxation of the x-axis being about an order of magnitude slower than that for the other two axes. On the other hand, the relatively symmetric NO_3 anion shows very isotropic rotation. As we discussed above, the self-diffusion coefficients of cation and anion in the ILs investigated were quite similar (deviating no more than 50% from each other). However, a strong decoupling of the cation and anion rotational dynamics can be seen from the data reported in Table 4. In [bmim][$N(CN)_2$], the anion's slowest relaxation time (τ_x) is about 4 times faster than the slowest rotation relaxation time for bmim, while relaxations for the other two axes are different almost by a factor of 10. Similarly, about 2 orders of magnitude difference between the rotational relaxations of the cation and anions is observed in [bmim][N_3] and about 3 orders in [bmim][NO_3]. The latter is due to exceptionally fast rotational dynamics of NO_3 as compared to other anions investigated here and is likely a consequence of the symmetric structure of NO_3 anion. Cadena and Maginn also analyzed the rotational dynamics of ions in their simulations of [bmim][NO_3].[23] Although they used a somewhat different definition of the molecular vector for which the rotational relaxation has been determined, the rotational relaxations obtained in their work for bmim are consistent with our data in Table 4. They found that the rotational relaxation of bmim changes from 2.5 ns at 298 K to about 100 ps at 393 K (the latter value was interpolated using the reported values at 363 and 423 K), while the average (over τ_x, τ_y, and τ_z) rotational relaxation from our simulations changed from 2.8 ns to 120 ps in the same temperature range. However, for the NO_3 anion, Cadena and Maginn reported rotational relaxation times of 91 ps at 298 K and about 3 ps at 393 K, while our simulations predict 6 and 1.8 ps relaxation times at 298 and 363 K, respectively.

It is also interesting to compare the temperature dependence of the rotational and translational motion, and thus to investigate the coupling of rotational and translational dynamics as a function of temperature. In Figure 9 we show the temperature dependence of $\tau_i D$, where τ_i are the rotational relaxation times from Table 4 ($i = x$, y, or z) and D is the ion self-diffusion coefficient from Table 3. Taking into account that rotational relaxation times are inversely proportional to the molecule rotational diffusion coefficient ($\tau_i \approx 1/D_r$) and assuming that translational and rotational diffusion coefficients of ions of radius R are correlated with the liquid viscosity (η) through the Stokes−Einstein[42] ($D = k_B T/(6\pi\eta R)$) and the Stokes−Einstein−Debye[43] relations ($D_r = k_B T/(8\pi\eta R^3)$), respectively, simple algebraic manipulations suggest that D_r/D, and hence $\tau_i D$, should be a constant, indicating that the rotational dynamics as a function of temperature changes the same way as the translational dynamics (i.e., the activation energies for these

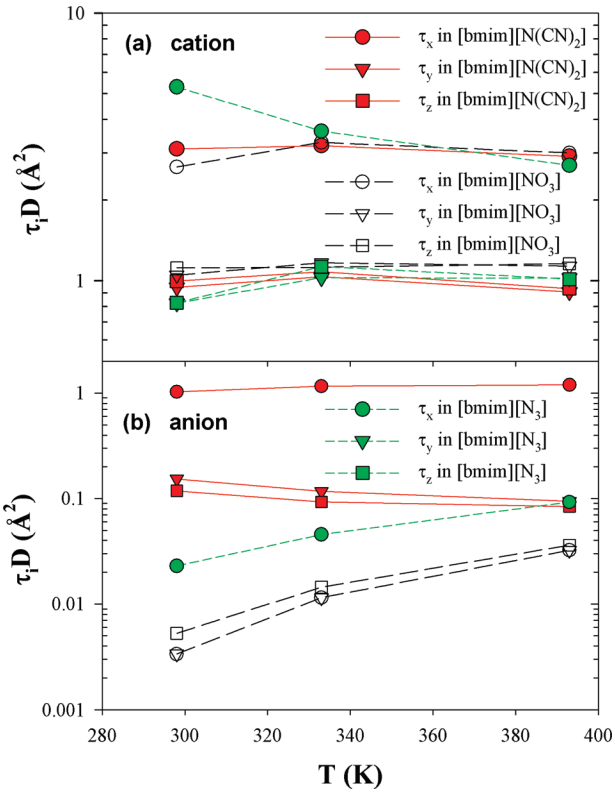

Figure 9. Temperature dependence of the product of rotational relaxation time (τ_i) and the ion self-diffusion coefficient (D) for (a) cation and (b) anion.

types of motion are the same). As can be seen in Figure 9a, this is mostly the case for bmim in the three ILs investigated. However, for anions, whose $\tau_i D$ are shown in Figure 9b, only $N(CN)_2$ shows this temperature independence (or weak dependence) of $\tau_i D$, while N_3 and NO_3 show strong temperature dependences, indicating that these anions have quite different temperature scaling for rotational and translational dynamics. Indeed values in Tables 3 and 4 show that, for example, the self-diffusion coefficient of NO_3 increases by a factor of 30 upon heating from 298 to 393 K, while the rotational dynamics speeds up only by a factor of 3−4 in the same temperature range. A similar rotational−translational decoupling, albeit to a smaller extent, has been observed in our simulations of ILs with another small anion bis(fluorosulfonyl)imide (FSI), while a larger bis(trifluoromethylsulfonyl)imide (Ntf_2) anion showed good coupling between rotational and translational motions in the temperature range 298−393 K.[44]

Other interesting information that can be obtained from Figure 9 is the average value of the ion MSD on the time scale corresponding to the rotational relaxation time for a given axis ($MSD_\tau = 6\tau_i D$). Figure 9a reveals that on the bmim τ_x time scale, the cation center-of-mass MSD_τ is about 18 Å^2, indicating that bmim has to move out of its intermolecular "cage" before rotational relaxation of the x-axis (see Figure 1 for definition) occurs. On the other hand, for bmim τ_y and τ_z, the corresponding $MSD_\tau \approx 6$ Å^2, which is noticeably smaller than the dimensions of bmim molecule. This indicates that the rotational relaxation of these axes can occur without significant translational motion of the molecule, that is, without leaving the cage. Similar analyses for the anions show that only rotation of $N(CN)_2$ around its largest dimension (x-direction) requires any noticeable displacement of the ion ($MSD_\tau \approx 6$ Å^2). For all other anions and rotational axes, the rotational relaxation can occur with minimal translational motion of the ion. This is particularly apparent at 298 K where MSD_τ values less than 0.1 Å^2 are required for rotational relaxation of N_3 and NO_3 anions. While this result can be expected for NO_3 due to its symmetric structure, the result is somewhat surprising for the linear N_3 anion. One might expect that formation of two relatively strong hydrogen bonds by the N_3 ends with the surrounding bmim molecules would interfere with the N_3 rotation, and, therefore, the rotation of this anion would be coupled to structural rearrangement in the system (i.e., translational motion of ions). This is clearly not the case, indicating that the formed hydrogens bonds between N_3 and bmim, while strong, are not long-lived. The latter might be due to availability of other hydrogen-bonding sites on bmim ring that can exchange the hydrogen bonding with the N_3 nitrogen without relaxation of intermolecular cage.

Finally, the ionic conductivity (λ) was calculated for each IL using the approach described in ref 28 and is also given in Table 1. In the ILs investigated, the degree of ion dynamic dissociation, as defined in ref 28, was around 0.6, and therefore trends in ionic conductivities obtained from simulations strongly correlate with those observed above for the self-diffusion coefficients. Table 1 also reports experimental conductivities available in the literature for [bmim][N(CN)$_2$].[45] A very good agreement between the simulation data and experiment for this IL further validates the quality of the APPLE&P force field and provides confidence in simulation predictions reported here for which no experimental data are available.

IV. Conclusions

Molecular dynamics simulations using the polarizable APPLE&P force field were conducted to investigate the influence of anion type on properties of [bmim]-based ILs. We have focused on ILs with relatively small, nitrogen-containing anions such as nitrate [NO_3], azide [N_3], and dicyanamide [$N(CN)_2$]. We found that the IL containing the $N(CN)_2$ anion shows noticeably different density, heat of vaporization, and ion binding energy as compared to the ILs with N_3 and NO_3 anions. Our simulations showed that [bmim][N_3] has the largest heat of vaporization while [bmim]$N(CN)_2$] has the smallest, a trend that is qualitatively different from the predictions of some empirical correlations reported in the literature, but consistent with ion binding energies obtained from the high-level quantum chemistry calculations. We also found that the cation−anion center-of-mass pair distribution function in the IL with the $N(CN)_2$ showed weaker correlations than the other two ILs. On the other hand, analysis of the three-dimensional density distributions of anion atoms around the cation showed that the preferable anion−cation coordination is independent of the anion type. Analysis of the butyl end-group distribution showed a small tendency for its aggregation independent of anion type. However, the extent of such aggregation observed in our simulations was found to be significantly smaller than what has been previously reported in the literature for [bmim][NO_3] using coarse-grained simulations. Analysis of ion dynamics showed that the highest ion mobility is observed in [bmim][N(CN)$_2$], consistent with the lowest heat of vaporization predicted for this IL. Rotational dynamics of the anions was found to be decoupled from ions translational motion, therefore allowing significant rotational relaxation with minimal translational motion of the ions.

As we mentioned in the Introduction, investigated ILs have been considered as potential new hypergolic liquids. However, only [bmim][N(CN)$_2$] IL mixed with common oxidizers showed a hypergolic behavior, while two other ILs were found nonhy-

pergolic. Interestingly, our simulations also showed that [bmim]-[$N(CN)_2$] has a number of thermophysical characteristics that are noticeably different from the other two ILs. It is tempting to try to correlate the differences observed in our simulations with trends in hypergolic behavior of these ILs. For example, one can speculate that the weaker ion−ion structural correlation observed in the [bmim][$N(CN)_2$] can ease the interaction/coordination of anion (the primary reactant in IL fuels) with/by oxidizer molecules and, hence, facilitate initial reactions between anion and oxidizer molecules, or that the faster ion mobility (i.e., lower viscosity) of the [bmim][$N(CN)_2$] can result in a higher mixing rate between the oxidizer and IL fuel and, hence, lead to more intense reactions. However, understanding the behavior of any hypergolic system is very challenging and complicated due to the large manifold of reactions involved and complex interplay between thermophysical properties (including those studied in this paper) and kinetics. Therefore, while we are confident that the reported in this work bulk properties and trends of ILs are certainly relevant to the ILs hypergolic behavior, we believe that any attempts to establish direct correlation only between the IL bulk properties and hypergolicity would be premature. We believe that investigation of thermophysical and reactive characteristics of IL/oxidizer mixtures has to be taken into account to obtain reliable correlations.

Acknowledgment. We are grateful for the financial support of this work by the Air Force Office of Scientific Research and the Air Force through STTR and SBIR programs (contract numbers FA9550-09-C-0110 and FA8650-09-M-2036, respectively) to Wasatch Molecular Inc. Opinions, interpretations, conclusions, and recommendations are those of the authors and are not necessarily endorsed by the United States Government. We also would like to thank Dr. G. L. Vaghjiani for technical discussions and manuscript preparation.

Supporting Information Available: Optimal low energy geometries as obtained from quantum chemistry calculations for ionic pairs, with several key atom−atom separations. Form of the tapering function for induced dipole−dipole interactions. This material is available free of charge via the Internet at http://pubs.acs.org.

References and Notes

(1) Forsyth, S. A.; Pringle, J. M.; MacFarlane, D. R. *Aust. J. Chem.* **2004**, *57*, 113.
(2) Jin, C. M.; Ye, C. F.; Phillips, B. S.; Zabinski, J. S.; Liu, X. Q.; Liu, W. M.; Shreeve, J. M. *J. Mater. Chem.* **2006**, *16*, 1529.
(3) Zeng, Z.; Phillips, B. S.; Xiao, J. C.; Shreeve, J. M. *Chem. Mater.* **2008**, *20*, 2719.
(4) Shin, J. H.; Henderson, W. A.; Passerini, S. *Electrochem. Commun.* **2003**, *5*, 1016.
(5) Garcia, B.; Lavallee, S.; Perron, G.; Michot, C.; Armand, M. *Electrochim. Acta* **2004**, *49*, 4583.
(6) Galinski, M.; Lewandowski, A.; Stepniak, I. *Electrochim. Acta* **2006**, *51*, 5567.
(7) De Long, H. C.; Trulove, P. C.; Sutto, T. E. *ACS Symp. Ser.* **2003**, *856*, 478.
(8) Ding, J.; Zhou, D.; Spinks, G.; Wallace, G.; Forsyth, S.; Forsyth, M.; MacFarlane, D. *Chem. Mater.* **2003**, *15*, 2392.
(9) Cho, M. S.; Seo, H. J.; Nam, J. D.; Choi, H. R.; Koo, J. C.; Song, K. G.; Lee, Y. *Sens. Actuators, B* **2006**, *119*, 621.
(10) Liu, Y.; Shi, L. H.; Wang, M. J.; Li, Z. Y.; Liu, H. T.; Li, J. H. *Green Chem.* **2005**, *7*, 655.
(11) Hough, W. L.; Rogers, R. D. *Bull. Chem. Soc. Jpn.* **2007**, *80*, 2262.
(12) Marsh, K. N.; Deev, A.; Wu, A. C. T.; Tran, E.; Klamt, A. *Korean J. Chem. Eng.* **2002**, *19*, 357.
(13) Schneider, S.; Hawkins, T.; Rosander, M.; Vaghjiani, G.; Chambreau, S.; Drake, G. *Energy Fuels* **2008**, *22*, 2871.
(14) Schneider, S.; Hawkins, T.; Rosander, M.; Mills, J.; Brand, A.; Hudgens, L.; Warmoth, G.; Vij, A. *Inorg. Chem.* **2008**, *47*, 3617.
(15) Schneider, S.; Hawkins, T.; Rosander, M.; Mills, J.; Vaghjiani, G.; Chambreau, S. *Inorg. Chem.* **2008**, *47*, 6082.
(16) Gao, H. X.; Joo, Y. H.; Twamley, B.; Zhou, Z. Q.; Shreeve, J. M. *Angew. Chem., Int. Ed.* **2009**, *48*, 2792.
(17) Micaelo, N. M.; Baptista, A. M.; Soares, C. M. *J. Phys. Chem. B* **2006**, *110*, 14444.
(18) Sambasivarao, S. V.; Acevedo, O. *J. Chem. Theory Comput.* **2009**, *5*, 1038.
(19) Kowsari, M. H.; Alavi, S.; Ashrafizaadeh, M.; Najafi, B. *J. Chem. Phys.* **2008**, *129*, 224508.
(20) Kowsari, M. H.; Alavi, S.; Ashrafizaadeh, M.; Najafi, B. *J. Chem. Phys.* **2009**, *130*, 014703.
(21) Feng, G.; Zhang, J. S.; Qiao, R. *J. Phys. Chem. C* **2009**, *113*, 4549.
(22) Wang, J.; Voth, G. A. *J. Am. Chem. Soc.* **2005**, *127*, 12192.
(23) Cadena, C.; Maginn, E. J. *J. Phys. Chem. B* **2006**, *110*, 18026.
(24) Emel'yanenko, V. N.; Verevkin, S. P.; Heintz, A.; Schick, C. *J. Phys. Chem. B* **2008**, *112*, 8095.
(25) Schroder, C.; Steinhauser, O. *J. Chem. Phys.* **2008**, *128*, 224503.
(26) Schroder, C.; Steinhauser, O. *J. Chem. Phys.* **2009**, *131*, 114504.
(27) Schroder, C.; Haberler, M.; Steinhauser, O. *J. Chem. Phys.* **2008**, *128*, 134501.
(28) Borodin, O. *J. Phys. Chem. B* **2009**, *113*, 11463.
(29) Hooper, J. B.; Borodin, O. *Phys. Chem. Chem. Phys.* **2010**, *12*, 4635.
(30) Starovoytov, O.; Borodin, O.; Hooper, J. B., in preparation.
(31) http://www.eng.utah.edu/~gdsmith/lucretius.html.
(32) Palmer, B. J. *J. Comput. Phys* **1993**, *104*, 470.
(33) Martyna, G. J.; Tuckerman, M. E.; Tobias, D. J.; Klein, M. L. *Mol. Phys.* **1996**, *87*, 1117.
(34) Fredlake, C. P.; Crosthwaite, J. M.; Hert, D. G.; Aki, S.; Brennecke, J. F. *J. Chem. Eng. Data* **2004**, *49*, 954.
(35) Seddon, K. R.; Stark, A.; Torres, M. J. *Clean Solvents* **2002**, *819*, 34.
(36) Blanchard, L. A.; Gu, Z. Y.; Brennecke, J. F. *J. Phys. Chem. B* **2001**, *105*, 2437.
(37) Emel'yanenko, V. N.; Verevkin, S. P.; Heintz, A. *J. Am. Chem. Soc.* **2007**, *129*, 3930.
(38) Chambreau, S. D.; Vaghjiani, G. L.; To, A.; Koh, C.; Strasser, D.; Kostko, O.; Leone, S. R. *J. Phys. Chem. B* **2010**, *114*, 1361.
(39) Verevkin, S. P. *Angew. Chem., Int. Ed.* **2008**, *47*, 5071.
(40) Borodin, O. *J. Phys. Chem. B* **2009**, *113*, 12353.
(41) Andriyko, Y. O.; Reischl, W.; Nauer, G. E. *J. Chem. Eng. Data* **2009**, *54*, 855.
(42) Einstein, A. *Investigations on the Theory of the Brownian Motion*; Dover: New York, 1956.
(43) Debye, P. *Polar Molecules*; Dover: New York, 1929.
(44) Borodin, O.; Gorecki, W.; Smith, G. D.; Armand, M. *J. Phys. Chem. B* **2010**, *114*, 6786.
(45) Yoshida, Y.; Baba, O.; Saito, G. *J. Phys. Chem. B* **2007**, *111*, 4742.

JP1049827